



ELSEVIER

Available online at [www.sciencedirect.com](http://www.sciencedirect.com)

SCIENCE @ DIRECT®

Journal of Constructional Steel Research 61 (2005) 1692–1712

JOURNAL OF  
CONSTRUCTIONAL  
STEEL RESEARCH

[www.elsevier.com/locate/jcsr](http://www.elsevier.com/locate/jcsr)

# Finite element analysis of CFT columns subjected to an axial compressive force and bending moment in combination

Hsuan-Teh Hu<sup>a,\*</sup>, Chiung-Shiann Huang<sup>b</sup>, Zhi-Liang Chen<sup>a</sup>

<sup>a</sup>*Department of Civil Engineering, National Cheng Kung University, Tainan, Taiwan, ROC*

<sup>b</sup>*Department of Civil Engineering, National Chiao Tung University, Hsinchu, Taiwan, ROC*

Received 12 March 2004; accepted 3 May 2005

---

## Abstract

Proper material constitutive models for concrete-filled tube (CFT) columns subjected to an axial compressive force and bending moment in combination are proposed and verified in this paper by using the nonlinear finite element program ABAQUS compared against experimental data. In the numerical analysis, the cross sections of the CFT columns are categorized into three groups, i.e., ones with circular sections, ones with square sections, and ones with square sections stiffened with reinforcing ties.

It is shown that the steel tubes can provide a good confining effect on the concrete core when the axial compressive force is large. The confining effect of a square CFT stiffened by reinforcing ties is stronger than that of the same square CFT without stiffening ties but weaker than that of a circular CFT. Nevertheless, when the spacing of reinforcing ties is small, a CFT with a square section might possibly achieve the same confining effect as one with a circular section.

© 2005 Elsevier Ltd. All rights reserved.

*Keywords:* Concrete-filled tube columns; Width-to-thickness ratio; Lateral confining pressure

---

---

\* Corresponding author. Tel.: +886 6 2757575x63168; fax: +886 6 2358542.

E-mail address: [hthu@mail.ncku.edu.tw](mailto:hthu@mail.ncku.edu.tw) (H.-T. Hu).

## 1. Introduction

A concrete-filled tube (CFT) column consists of a steel tube filled with concrete. The concrete core adds stiffness and compressive strength to the tubular column and reduces the potential for inward local buckling. On the other hand, the steel tube acts as longitudinal and lateral reinforcement for the concrete core helping it to resist tension, bending moment, and shear and helping to prevent the concrete from spalling. Due to the benefit of composite action of the two materials, the CFT columns provide excellent seismic event resistant structural properties such as high strength, high ductility and large energy absorption capacity. In addition, the steel tube acts as both erection steel and forming for the composite column during construction; thus a considerable amount of labor, materials and construction cost can be avoided. As a result, CFT columns have gained popularity in supporting heavy loads in high rise buildings, bridges and offshore structures. Various experimental and analytical studies have been performed on CFT columns [1–19].

It is known that the ultimate strengths of CFT columns are influenced by their constituent material properties such as the compressive strength of the concrete, the yield strength of the steel, and the nonlinear behaviors of these two materials. In addition, the ultimate strengths of CFT columns are also influenced by the concrete confining pressure and the geometric properties of the tubes, such as the shape of the cross section, the width-to-thickness ratio, and the spacing and the diameter of the reinforcing ties. With all of these factors having effects, how one predicts the ultimate strengths of CFT columns accurately requires more thorough study.

In this paper, appropriate nonlinear constitutive material models for steel reinforcing ties, steel tubes and confined concrete are proposed. Then, the nonlinear finite element program ABAQUS [20] is employed to perform numerical simulations of CFT columns subjected to combined axial compressive forces and bending moments. The proposed material constitutive models as well as the predicted ultimate strengths of CFT columns are verified against experimental data of Liu et al. [21]. Finally, the influence of the concrete confining pressure and the geometric properties of the columns on the behavior of CFT columns are studied and discussed.

## 2. Material properties and constitutive models

The cross sections of the CFT columns in this investigation are categorized into three groups (Fig. 1), i.e., ones with circular sections (denoted by CU), ones with square sections (denoted by SU), and ones with square sections stiffened with steel reinforcing ties forming an octagonal shape (denoted by SS). The square tubes with the SU sections were constructed by seam welding two U-shaped cold-formed steel plates. If stiffening was specified for SS sections, the tie bars with circular cross section were fillet welded to the U-shaped cold-formed steel plates before making the seam complete-penetration groove welds [21]. The materials used in the numerical analysis involve steel reinforcing ties (for SS sections only), steel tubes and concrete. Constitutive models of these materials are proposed and discussed as follows.

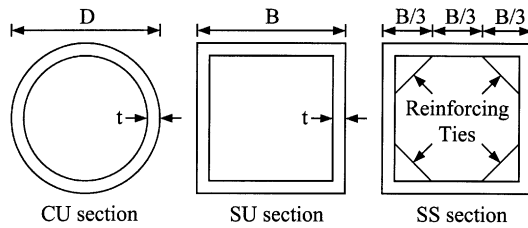


Fig. 1. Cross sections of CFT columns.

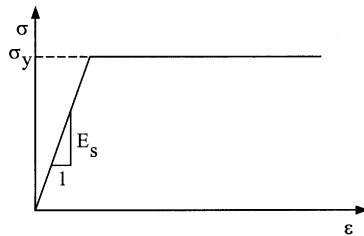


Fig. 2. Elastic–perfectly plastic stress–strain curve for steel.

### 2.1. Steel reinforcing ties

When the stress in a reinforcing tie exceeds the yield stress  $\sigma_y$ , the tie will exhibit plastic deformation. The stress–strain curve of the reinforcing tie is assumed to be an elastic–perfectly plastic one (Fig. 2). The elastic modulus of the reinforcing tie  $E_s$  is assumed to be equal to 200 GPa.

### 2.2. Steel tubes

In the analysis, the Poisson’s ratio  $\nu_s$  and the elastic modulus  $E_s$  of the steel tube are assumed to be 0.3 and 200 GPa, respectively. The uniaxial behavior of the steel tube is similar to that of the reinforcing tie and thus can be simulated by an elastic–perfectly plastic model. When the steel tube is subjected to multiple stresses, a von Mises yield criterion  $F$  is employed to define the elastic limit, which is written as

$$F = \sqrt{3J_2} = \frac{1}{\sqrt{2}}\sqrt{(\sigma_1 - \sigma_2)^2 + (\sigma_2 - \sigma_3)^2 + (\sigma_3 - \sigma_1)^2} = \sigma_y \tag{1}$$

where  $J_2$  is the second stress invariant of the stress deviator tensor and  $\sigma_1$ ,  $\sigma_2$ , and  $\sigma_3$  are the principal stresses. Fig. 3 shows the von Mises yield surface in the three-dimensional principal stress space. The response of the steel tube is modeled by an elastic–perfectly plastic theory with an associated flow rule. When the stress points fall inside the yield surface, the behavior of the steel tube is linearly elastic. If the stresses of the steel tube reach the yield surface, the behavior of the steel tube becomes perfectly plastic. Consequently, the steel tube is assumed to fail and cannot resist any further loading.

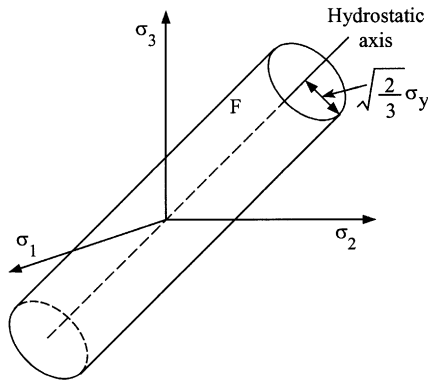


Fig. 3. von Mises yield surface in the three-dimensional principal stress space.

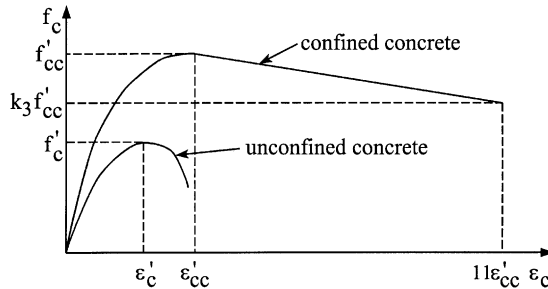


Fig. 4. Equivalent uniaxial stress–strain curve for concrete.

### 2.3. Concrete

The Poisson’s ratio  $\nu_c$  of concrete under uniaxial compressive stress ranges from 0.15 to 0.22, with a representative value of 0.19 or 0.20 [22]. In this study, the Poisson’s ratio of concrete is assumed to be 0.2.

Let the uniaxial compressive strength and the corresponding strain of the unconfined concrete be  $f'_c$  and  $\epsilon'_c$  (Fig. 4). The value of  $\epsilon'_c$  is usually around the range of 0.002–0.003. A representative value 0.002 is used in the analysis. When concrete is subjected to laterally confining pressure, the uniaxial compressive strength  $f'_{cc}$  and the corresponding strain  $\epsilon'_{cc}$  (Fig. 4) are much higher than those of unconfined concrete. The relations between  $f'_{cc}$ ,  $f'_c$  and between  $\epsilon'_{cc}$ ,  $\epsilon'_c$  are approximated by the following equations [23]:

$$f'_{cc} = k_4 f'_c + k_1 f_i \tag{2}$$

$$\epsilon'_{cc} = \epsilon'_c \left( 1 + k_2 \frac{f_i}{f'_c} \right) \tag{3}$$

where  $f_i$  represents the confining pressure around the concrete core.  $k_1$  and  $k_2$  are constants and can be obtained from experimental data. Meanwhile, the constants  $k_1$  and  $k_2$  were set as 4.1 and 20.5 on the basis of the studies of Richart et al. [24]. The original version of

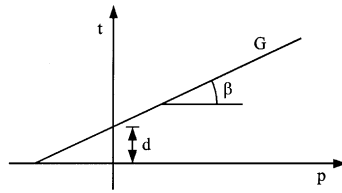


Fig. 5. Linear Drucker–Prager yield criterion for concrete.

Eq. (2) was proposed for concrete subjected to hydrostatic pressure [23] and did not contain the strength factor  $k_4$ . For a CFT subjected to a bending moment, part of the concrete may be subject to tensile stress, which is different from the hydrostatic pressure condition. Therefore, a strength factor  $k_4$  is introduced by the authors with the limitation  $k_4 \leq 1$ .

Because the concrete in the CFT columns is usually subjected to triaxial compressive stresses, the failure of concrete is dominated by the compressive failure surface expanding with increasing hydrostatic pressure. Hence, a linear Drucker–Prager yield criterion  $G$  (Fig. 5) is used to model the yield surface of concrete, which is expressed as

$$G = t - p \tan \beta - d = 0 \tag{4}$$

where

$$p = -(\sigma_1 + \sigma_2 + \sigma_3)/3 \tag{5a}$$

$$d = \left(1 - \frac{\tan \beta}{3}\right) f'_{cc} \tag{5b}$$

$$t = \frac{\sqrt{3}J_2}{2} \left[1 + \frac{1}{K} - \left(1 - \frac{1}{K}\right) \left(\frac{r}{\sqrt{3}J_2}\right)^3\right] \tag{5c}$$

$$r = \left[\frac{9}{2}(S_1^3 + S_2^3 + S_3^3)\right]^{1/3} \tag{5d}$$

and  $S_1$ ,  $S_2$ , and  $S_3$  are principal stress deviators. The constants  $K$  and  $\beta$  are material parameters determined from experimental data. In the analysis,  $K$  and  $\beta$  are set to 0.8 and  $20^\circ$ , respectively [25].

The response of the concrete is modeled by an elastic–plastic theory with associated flow and an isotropic hardening rule. When plastic deformation occurs, there should be a certain parameter to guide the expansion of the yield surface. A commonly used approach is to relate the multidimensional stress and strain conditions to a pair of quantities, namely, the effective stress  $f_c$  and effective strain  $\varepsilon_c$ , such that results obtained following different loading paths can all be correlated by means of the equivalent uniaxial stress–strain curve. The stress–strain relationship proposed by Saenz [26] has been widely adopted as the uniaxial stress–strain curve for concrete and it has the following form:

$$f_c = \frac{E_c \varepsilon_c}{1 + (R + R_E - 2) \left(\frac{\varepsilon_c}{\varepsilon_{cc}}\right) - (2R - 1) \left(\frac{\varepsilon_c}{\varepsilon_{cc}}\right)^2 + R \left(\frac{\varepsilon_c}{\varepsilon_{cc}}\right)^3} \tag{6}$$

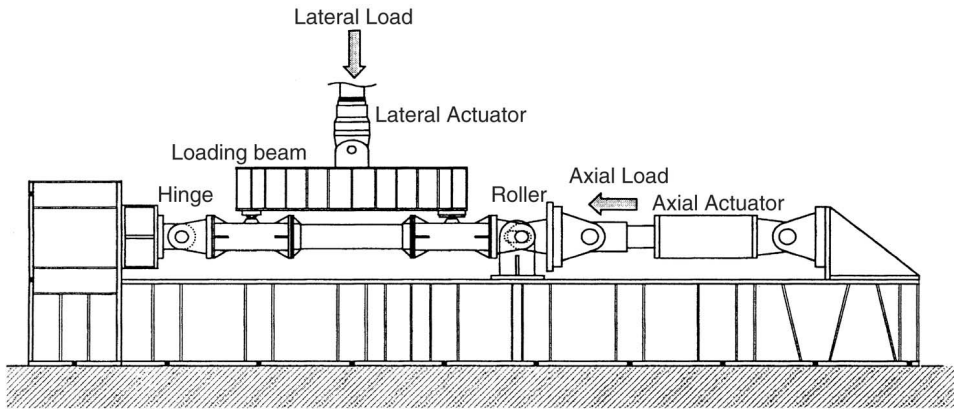


Fig. 6. Experimental set-up for a CFT column subjected to an axial compressive force and a moment in combination.

where

$$R = \frac{R_E(R_\sigma - 1)}{(R_E - 1)^2} - \frac{1}{R_E}, \quad R_E = \frac{E_c \varepsilon'_{cc}}{f'_{cc}}$$

and  $R_\sigma = 4$ ,  $R_E = 4$  may be used [27]. The initial modulus of elasticity of concrete  $E_c$  is highly correlated with its compressive strength and can be calculated with reasonable accuracy from the empirical equation [28]

$$E_c = 4700\sqrt{f'_{cc}} \text{ MPa}. \tag{7}$$

In the analysis, Eq. (6) is taken as the equivalent uniaxial stress–strain curve for concrete when the concrete strain  $\varepsilon_c$  is less than  $\varepsilon'_{cc}$  (Fig. 4). When  $\varepsilon_c > \varepsilon'_{cc}$ , a linear descending line is used to model the softening behavior of concrete. If  $k_3$  is defined as the material degradation parameter, the descending line is assumed to be terminated at the point where  $f_c = k_3 f'_{cc}$  and  $\varepsilon_c = 11\varepsilon'_{cc}$  [19].

Generally, the parameters  $f_t$ ,  $k_3$  and  $k_4$  should be provided in order to completely define the equivalent uniaxial stress–strain relation. These three parameters apparently depend on the cross-sectional shape and stiffening mean. Consequently, their appropriate values are determined by matching the numerical results with experimental data via a parametric study.

### 3. Finite element model for CFT columns

The experiment set-up for a CFT column subjected to an axial compressive force and a moment in combination carried out by Liu et al. [21] is shown in Fig. 6. The beam tested is simply supported at two ends and is composed of a CFT at the center portion and two rigid steel beams with stiffeners at the outer portions (Fig. 7(a)). The beam is compressed by a constant axial force  $F$  first. Then two concentrated lateral loads  $P$ , forming a four-point bend, are applied to the beam and gradually increased to the ultimate load.

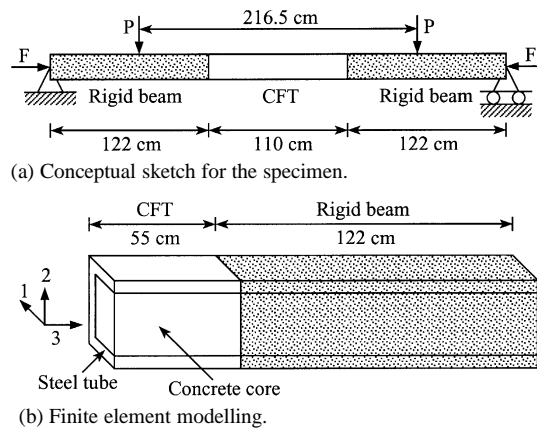


Fig. 7. Conceptual sketch and finite element modeling of a CFT column.

Due to symmetry, only a quarter of the CFT column is analyzed (Fig. 7(b)). Symmetric boundary conditions are imposed on the symmetric planes:  $u_3 = 0$  on the left surface of the element mesh and  $u_1 = 0$  on the front surface of the element mesh surface. To simulate the roller support, the displacements  $u_2$  for the nodes at the mid-depth of the right edge of the element mesh are all set to zero.

In the finite element mesh, both the concrete core and the steel tube are modeled by 27-node solid elements (three degrees of freedom per node) with a reduced integration rule. For the SS section, the steel reinforcing tie is modeled by 3-node truss elements. The rigid portion of the beam is also modeled by 27-node solid elements. However, its material behavior is assumed to be linear elastic with the elastic modulus  $E_r$  equal to  $1 \times 10^7$  GPa and Poisson's ratio  $\nu_r$  equal to 0.01. The interface between the concrete core and steel tube is modeled by a pair of contact surfaces. The nodes of the concrete core and the steel tube are connected through contact surfaces that require matching meshes of the two bodies. The contact surfaces can model infinitesimal sliding and friction [20] between the concrete core and steel tube. The friction coefficient used in all the analyses is 0.25. Through the contact surfaces, the concrete core and steel tube are allowed to either contact or separate but not to penetrate each other.

Convergent studies of the finite element meshes have been done by the author using various element sizes for CFT columns with CU and SU sections [25]. It is shown that the numerical results are not sensitive to the element sizes and mesh refinements. As a result, the meshes shown in Fig. 8 are used for CFT columns with CU, SU and SS sections throughout the analyses.

#### 4. Numerical analysis

In this section, the experimental data from Liu et al. [21] are used to verify and calibrate the proposed material model for CFT columns. For systemization, each specimen in the analysis has an individual designation, involving two English letters followed by a series

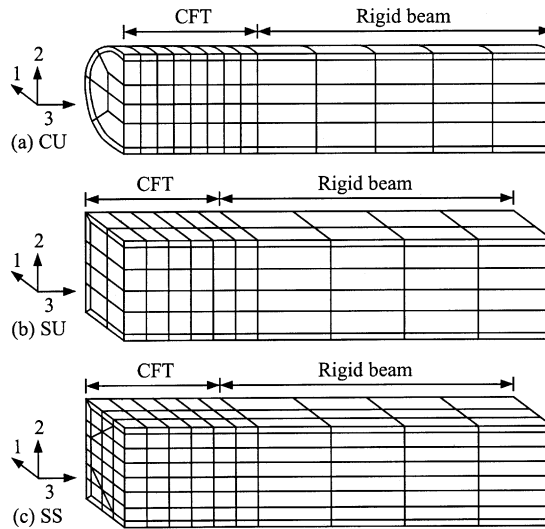


Fig. 8. Finite element meshes for CFT columns.

of numbers (Table 1). The first letter, C or S, represents the cross-sectional shape of the specimen (circular or square, respectively). The second letter, S or U, denotes a specimen with or without stiffening ties, respectively. Meanwhile, the number following the English letters denotes the axial load ratio  $F/F_u$  of the beam, where  $F_u$  is the axial load strength calculated by using Eurocode 4 [21,29]. For stiffened specimens, the last symbol, B/3 or B/5, represents the center-to-center spacing between the steel reinforcing ties and a unique size of tie bar (#3 bar with diameter 9.52 mm) is used.

#### 4.1. Simulations of CFT columns with CU sections

The results of numerical simulations for CFT columns with CU sections are given in Table 2. The curves of moment versus curvature at the mid-span of the beams are plotted against the experiment data in Fig. 9. Generally, the numerical results show good agreement with the experimental data. The moment–curvature curves of these CFT columns exhibit a very ductile behavior before the failure of the specimens occurs. This ductile behavior becomes more prominent when the axial load ratio  $F/F_u$  is small.

The values of  $f_l/f_y$ ,  $k_3$  and  $k_4$  versus the axial load ratio  $F/F_u$  for CFT columns with CU sections are shown in Fig. 10(a), (b) and (c), respectively. It can be observed from Fig. 10(a) that the axial load ratio  $F/F_u$  has significant influence on the lateral confining pressure  $f_l$ . When the axial load ratio  $F/F_u$  is less than 0.23, the steel tubes provide weak lateral support to the concrete core and the lateral confining pressure  $f_l$  applied to the concrete core is zero during the subsequent four-point bending loading. When the axial load ratio  $F/F_u$  is greater than 0.23, the steel tubes provide strong lateral support to the concrete core and the lateral confining pressure  $f_l$  increases with the increasing of the axial load ratio  $F/F_u$ . However, when the axial load ratio  $F/F_u$  is greater than 0.56, the

Table 1  
Geometry and material properties of CFT columns

Column no.	Axial force $F$ (kN)	$F_u$ (kN)	$D$ or $B$ (mm)	$t$ (mm)	$D/t$ or $B/t$	Length (mm)	Steel tube $f_y$ (MPa)	Concrete $f'_c$ (MPa)	Steel tie $f_y$ (MPa)
CU-0	0	2390	280	4	70	1100	285	24.2	–
CU-0.23	542	2390	280	4	70	1100	285	24.2	–
CU-0.34	812	2390	280	4	70	1100	285	24.2	–
CU-0.45	1200	2690	280	4	70	1100	288	29.1	–
CU-0.56	1354	2390	280	4	70	1100	285	24.2	–
CU-0.74	2000	2690	280	4	70	1100	288	29.1	–
SU-0	0	3050	280	4	70	1100	285	24.2	–
SU-0.23	800	3420	280	4	70	1100	288	29.1	–
SU-0.34	1035	3050	280	4	70	1100	285	24.2	–
SU-0.35	1200	3420	280	4	70	1100	288	29.1	–
SU-0.45	1378	3050	280	4	70	1100	285	24.2	–
SU-0.57	1725	3050	280	4	70	1100	285	24.2	–
SS-0-B/3	0	3050	280	4	70	1100	285	24.2	408
SS-0.23-B/3	800	3420	280	4	70	1100	288	29.1	468
SS-0.35-B/3	1200	3420	280	4	70	1100	288	29.1	468
SS-0.47-B/3	1600	3420	280	4	70	1100	288	29.1	468
SS-0.58-B/3	2000	3420	280	4	70	1100	288	29.1	468
SS-0-B/5	0	3420	280	4	70	1100	288	29.1	468
SS-0.23-B/5	800	3420	280	4	70	1100	288	29.1	468
SS-0.35-B/5	1200	3420	280	4	70	1100	288	29.1	468
SS-0.47-B/5	1600	3420	280	4	70	1100	288	29.1	468
SS-0.58-B/5	2000	3420	280	4	70	1100	288	29.1	468

increasing of the lateral confining pressure  $f_l$  is less sensitive to the  $F/F_u$  ratio. From the results of numerical simulations, empirical equations for  $f_l/f_y$  may be proposed as follows:

$$f_l/f_y = 0, \quad 0 \leq F/F_u \leq 0.23 \quad (8a)$$

$$f_l/f_y = -0.00859 + 0.0373(F/F_u), \quad 0.23 \leq F/F_u \leq 0.56 \quad (8b)$$

$$f_l/f_y = 0.0104 + 0.00333(F/F_u), \quad 0.56 \leq F/F_u \leq 0.74. \quad (8c)$$

From Fig. 10(b), we can see that the material degradation parameter  $k_3$  generally decreases with the increasing of the axial load ratio  $F/F_u$ . However, when the axial load ratio  $F/F_u$  is greater than 0.56, the influence of the  $F/F_u$  ratio on the parameter  $k_3$  seems to be less significant. On the basis of the results of numerical simulations, the empirical equations for  $k_3$  may be proposed as follows:

$$k_3 = 1 - 0.304(F/F_u), \quad 0 \leq F/F_u \leq 0.23 \quad (9a)$$

$$k_3 = 1.195 - 1.152(F/F_u), \quad 0.23 \leq F/F_u \leq 0.56 \quad (9b)$$

$$k_3 = 0.55, \quad 0.56 \leq F/F_u \leq 0.74. \quad (9c)$$

From Fig. 10(c), we can see that the strength factor  $k_4$  is less than 1 when the axial load ratio  $F/F_u$  is less than 0.23. This might mean that when the axial compressive load is small,

Table 2  
Results of numerical analyses

Column no.	Ultimate moment (kN m)		Error (%)	$f_l$ (MPa)	$f_l/f_y$	$k_3$	$k_4$
	Experiment	Analysis					
CU-0	131.8	131.7	0.08	0.00	0.0000	1.00	0.70
CU-0.23	154.6	153.8	0.52	0.00	0.0000	0.93	1.00
CU-0.34	164.3	161.4	1.77	1.33	0.0047	0.75	1.00
CU-0.45	182.3	182.1	0.11	2.58	0.0090	0.65	1.00
CU-0.56	171.8	171.9	0.06	3.50	0.0123	0.55	1.00
CU-0.74	161.9	159.5	1.48	3.70	0.0129	0.61	1.00
SU-0	169.1	171.7	1.54	0.00	0.0000	0.87	0.47
SU-0.23	225.9	222.9	1.33	0.00	0.0000	0.63	0.88
SU-0.34	200.3	197.4	1.45	0.00	0.0000	0.55	0.97
SU-0.35	231.2	228.0	1.38	0.30	0.0010	0.50	1.00
SU-0.45	220.6	220.6	0.00	0.70	0.0025	0.47	1.00
SU-0.57	186.2	183.7	1.34	1.00	0.0035	0.46	1.00
SS-0-B/3	178.2	179.3	0.62	0.00	0.0000	0.93	0.50
SS-0.23-B/3	237.3	238.4	0.46	0.00	0.0000	0.88	0.90
SS-0.35-B/3	256.5	257.2	0.27	1.05	0.0036	0.70	1.00
SS-0.47-B/3	240.2	237.9	0.96	1.30	0.0045	0.35	1.00
SS-0.58-B/3	240.4	238.9	0.62	2.30	0.0080	0.35	1.00
SS-0-B/5	211.3	214.6	1.56	0.00	0.0000	1.00	0.70
SS-0.23-B/5	254.3	255.8	0.59	0.00	0.0000	0.96	0.93
SS-0.35-B/5	277.1	276.0	0.40	1.20	0.0042	0.90	1.00
SS-0.47-B/5	279.9	281.4	0.54	2.65	0.0092	0.68	1.00
SS-0.58-B/5	276.4	276.4	0.00	3.40	0.0118	0.55	1.00

part of the concrete core is subjected to tensile stress during the four-point bending. With weak later support from the steel tube, this part of the concrete is prone to crack easily. On average, the entire concrete cross section cannot maintain the strength  $f'_c$  and the strength factor  $k_4$  is thus less than 1. When the axial compressive load is large (e.g.  $F/F_u > 0.23$ ), the concrete core has strong lateral support from the steel tube and is not prone to cracking. As a result, the strength factor  $k_4$  is set to the limit value 1. On the basis of the results of numerical simulations, the empirical equations for  $k_4$  may be proposed as follows:

$$k_4 = 0.7 + 1.304(F/F_u), \quad 0 \leq F/F_u \leq 0.23 \quad (10a)$$

$$k_4 = 1, \quad 0.23 \leq F/F_u. \quad (10b)$$

Fig. 11(a) shows the typical deformation shapes of CU-0.34 column around the ultimate loading stage. It can be observed that the concrete core and steel tube keep in contact with each other and no local buckling of the tube takes place. This phenomenon can also be observed for CFT columns with CU sections at other axial load ratios [25].

#### 4.2. Simulations of CFT columns with SU sections

The results of numerical simulations for CFT columns with SU sections are also shown in Table 2. The curves of moment versus curvature at the mid-span of the beams are plotted

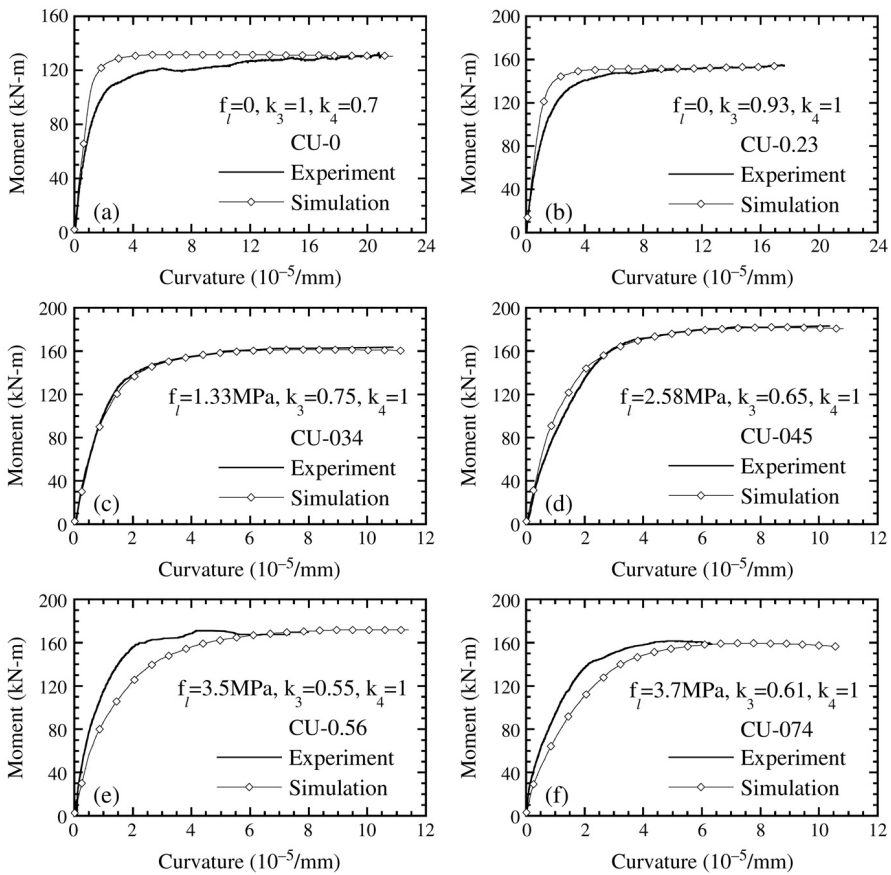


Fig. 9. Moment versus curvature for CFT columns with CU sections.

against the experiment data in Fig. 12. Generally, the numerical results show good agreement with the experimental data. The moment–curvature curves of these CFT columns only exhibit a ductile behavior when the axial load ratio  $F/F_u$  is close to zero. With increasing of the axial load ratio, the CFT columns can no longer maintain their strength after the ultimate moment capacities have been reached. As a result, the moment–curvature curves of these specimens start to descend after the peak moments have been reached. This descending phenomenon is more prominent when the axial load ratio is large.

The values of  $f_l/f_y$ ,  $k_3$  and  $k_4$  versus axial load ratio  $F/F_u$  for CFT columns with SU sections are shown in Fig. 13(a), (b) and (c), respectively. From Fig. 13(a), we can see that when the axial load ratio  $F/F_u$  is less than 0.34, the lateral confining pressure  $f_l$  applied to the concrete core is zero. When the axial load ratio  $F/F_u$  is greater than 0.34, the steel tubes start to provide lateral support to the concrete core and the lateral confining pressure  $f_l$  increases with the increasing of the axial load ratio  $F/F_u$ . By comparing Fig. 13(a) with Fig. 10(a), one can observe that the lateral confining pressure  $f_l$  for a CFT column with the

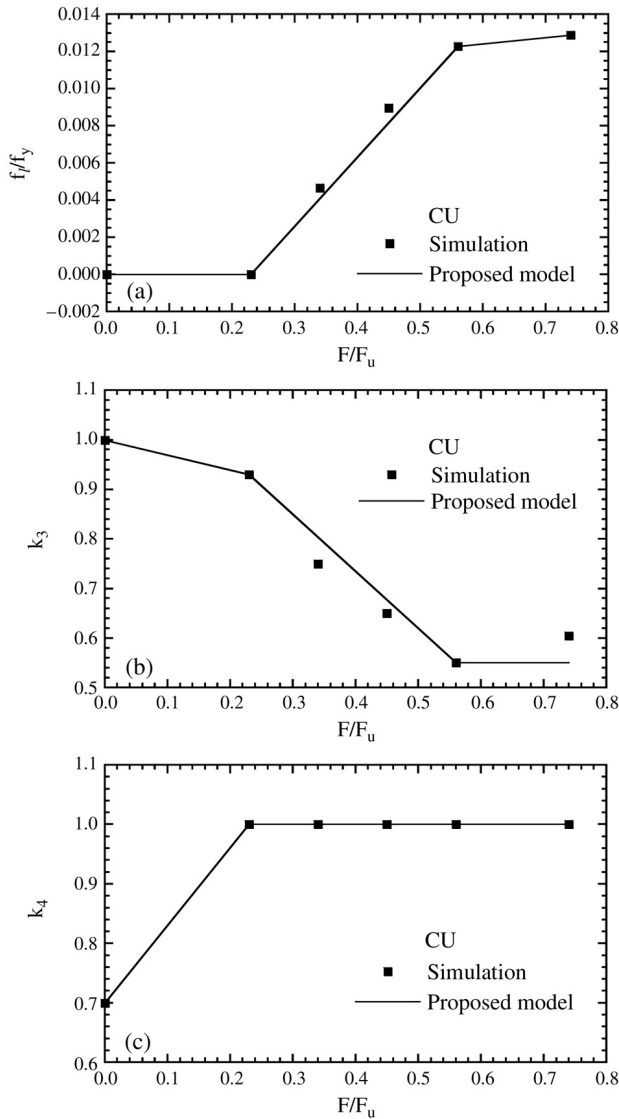


Fig. 10.  $f_l/f_y$ ,  $k_3$  and  $k_4$  versus axial load ratio  $F/F_u$  for CFT columns with CU section.

SU section is much less than that for a CFT column with the CU section. Even when the axial load ratio  $F/F_u$  is 0.57, the value of the  $f_l/f_y$  ratio for a CFT column with the SU section is only about 1/4 of that for a CFT column with the CU section. From the results of numerical simulations, the empirical equations for  $f_l/f_y$  may be proposed as follows:

$$f_l/f_y = 0, \quad 0 \leq F/F_u \leq 0.34 \tag{11a}$$

$$f_l/f_y = -0.00517 + 0.0152(F/F_u), \quad 0.34 \leq F/F_u \leq 0.57. \tag{11b}$$

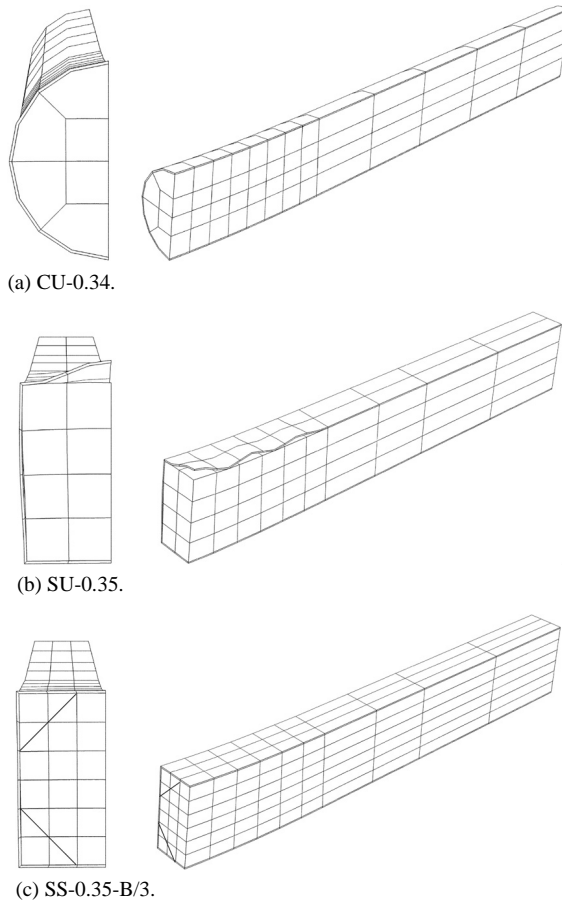


Fig. 11. Deformation shapes of CFT columns.

From Fig. 13(b), we can see again that the material degradation parameter  $k_3$  decreases with increasing values of the axial load ratio  $F/F_u$ . When the axial load ratio  $F/F_u$  is greater than 0.45, the decreasing of the material degradation parameter  $k_3$  is less sensitive to the  $F/F_u$  ratio. By comparing Fig. 13(b) with Fig. 10(b), one can observe that the material degradation parameter  $k_3$  for a CFT column with the SU section is also smaller than that for a CFT column with the CU section subjected to the same axial load ratio. This means that the strength of concrete in the SU section case degrades more than that in the CU section case. This can be explained as the CFT tubes with SU sections providing weaker lateral support to concrete core than those with CU sections. From the results of numerical simulations, the empirical equations for  $k_3$  may be proposed as follows:

$$k_3 = 0.87 - 0.889(F/F_u), \quad 0 \leq F/F_u \leq 0.45 \quad (12a)$$

$$k_3 = 0.508 - 0.083(F/F_u), \quad 0.45 \leq F/F_u \leq 0.57. \quad (12b)$$

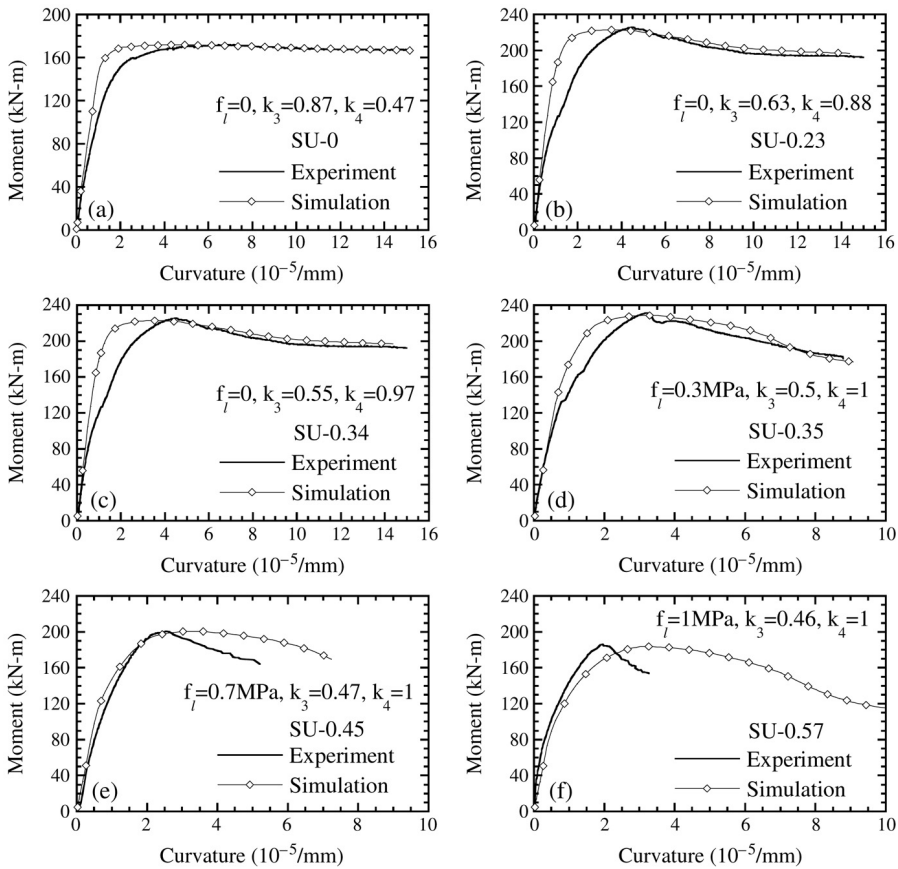


Fig. 12. Moment versus curvature for CFT columns with SU sections.

From Fig. 13(c), it is shown that the strength factor  $k_4$  is less than 1 when the axial load ratio  $F/F_u$  is less than 0.35. By comparing Fig. 13(c) with Fig. 10(c), we can see that with  $F/F_u < 0.23$ , the strength factor  $k_4$  for a CFT column with the SU section is usually smaller than that for one with the CU section subjected to the same axial load ratio. This is again due to the CFT tubes with SU sections providing weaker lateral support to concrete core than those with CU sections. On the basis of the results of numerical simulations, the empirical equations for  $k_4$  may be proposed as follows:

$$k_4 = 0.42 + 1.706(F/F_u), \quad 0 \leq F/F_u \leq 0.34 \tag{13a}$$

$$k_4 = 1, \quad 0.34 \leq F/F_u \leq 0.57. \tag{13b}$$

Fig. 11(b) shows the typical deformation shapes of SU-0.35 columns during the ultimate loading stage. It can be observed that the concrete core and steel tube cannot keep in contact to each other at the top and mid-span regions of the column where severe local buckling

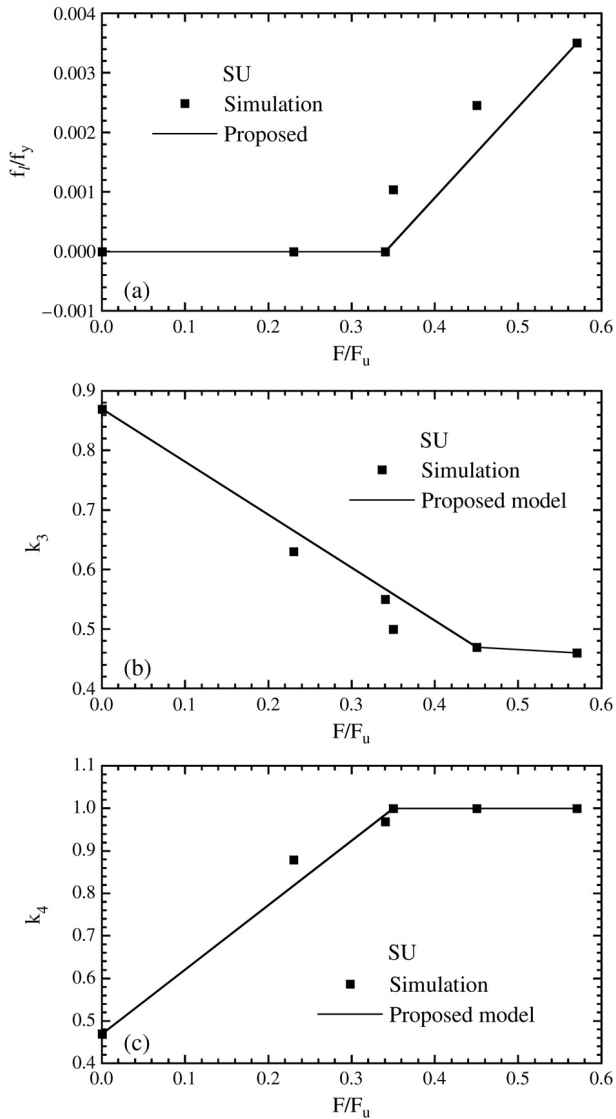


Fig. 13.  $f_t/f_y$ ,  $k_3$  and  $k_4$  versus axial load ratio  $F/F_u$  for CFT columns with SU sections.

of the tube takes place. This phenomenon can also be observed for the CFT with the SU section at other axial load ratios [25].

#### 4.3. Simulations of CFT columns with SS sections

The results of numerical simulations for CFT columns with SS sections are given in Table 2. The curves of axial force versus axial strain for these columns are plotted against

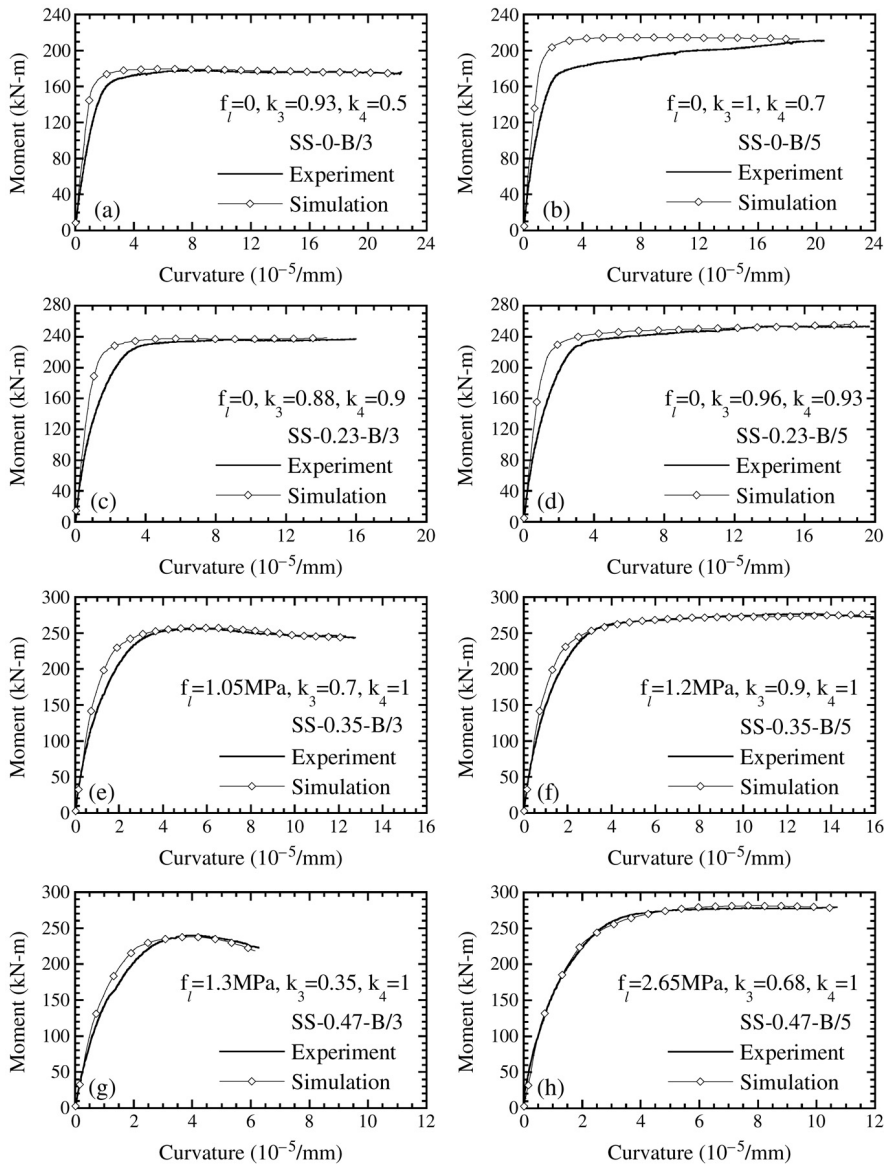


Fig. 14. Moment versus curvature for CFT columns with SS sections.

the experiment data in Fig. 14. Generally, the numerical results again show good agreement with the experimental data. When the spacing of reinforcing ties is small (e.g. B/5), the moment–curvature curves of these CFT columns exhibit a ductile behavior before the failure of the specimens occurs. This ductile behavior becomes more prominent when the axial load ratio  $F/F_u$  is small. When the spacing of reinforcing ties is large (e.g. B/3), the

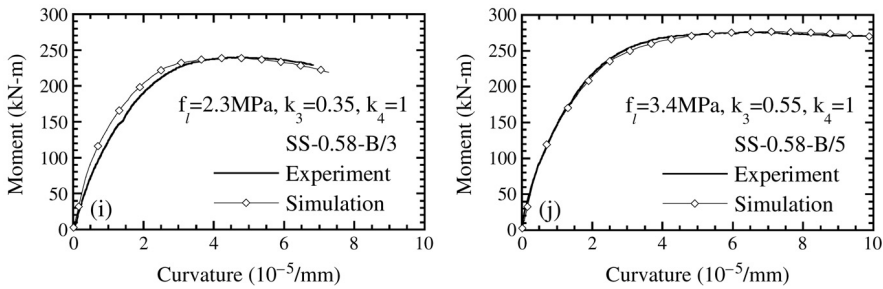


Fig. 14. (continued).

moment–curvature curves of the CFT columns exhibit a ductile behavior with a small axial load ratio (e.g.  $F/F_u < 0.23$ ). On the other hand, the moment–curvature curves of the CFT columns show a descending portion when the axial load ratio is large (e.g.  $F/F_u > 0.35$ ). This descending phenomenon is more prominent when the axial load ratio becomes large.

The values of  $f_l/f_y$ ,  $k_3$  and  $k_4$  versus axial load ratio  $F/F_u$  for CFT columns with SS sections are shown in Fig. 15(a), (b) and (c), respectively. From Fig. 15(a), we can see that when the axial load ratio  $F/F_u$  is less than 0.23, the lateral confining pressure  $f_l$  applied to the concrete core is zero. When the axial load ratio  $F/F_u$  is greater than 0.23, the steel tubes start to provide lateral support to the concrete core and the lateral confining pressure  $f_l$  increases with the increasing of the axial load ratio  $F/F_u$ . For a CFT with reinforcing ties at close spacing (e.g. B/5), the lateral confining pressure  $f_l$  is usually greater than that with reinforcing ties at large spacing (e.g. B/3). By comparing Fig. 15(a) with Figs. 13(a) and 10(a), one can observe that the lateral confining pressure  $f_l$  for the CFT column with the SS section is much higher than that for one with the SU section and is of about the same order as that for one with the CU section. This proves that the use of reinforcing ties enhances the lateral confining pressure of the square tubes. From the results of numerical simulations, the empirical equations for  $f_l/f_y$  may be proposed when the reinforcing ties are at B/3 spacing:

$$f_l/f_y = 0, \quad 0 \leq F/F_u \leq 0.23 \quad (14a)$$

$$f_l/f_y = -0.00527 + 0.0229(F/F_u), \quad 0.23 \leq F/F_u \leq 0.58. \quad (14b)$$

When reinforcing ties are at B/5 spacing, the following equations may be suggested:

$$f_l/f_y = 0, \quad 0 \leq F/F_u \leq 0.23 \quad (15a)$$

$$f_l/f_y = -0.00775 + 0.0337(F/F_u), \quad 0.23 \leq F/F_u \leq 0.58. \quad (15b)$$

From Fig. 15(b), we can see again that the material degradation parameter  $k_3$  decreases with increasing value of the axial load ratio  $F/F_u$ . For a CFT with reinforcing ties at close spacing (e.g. B/5), the material degradation parameter  $k_3$  is usually greater than that for a CFT with reinforcing ties at large spacing (e.g. B/3) due to the enhancement of the lateral confining effect. By comparing Fig. 15(b) with Figs. 13(b) and 10(b), one can observe that with the same axial load ratio, the material degradation parameter  $k_3$  for a CFT with the SS section is larger than that for a CFT with the SU section but smaller than that for a CFT with

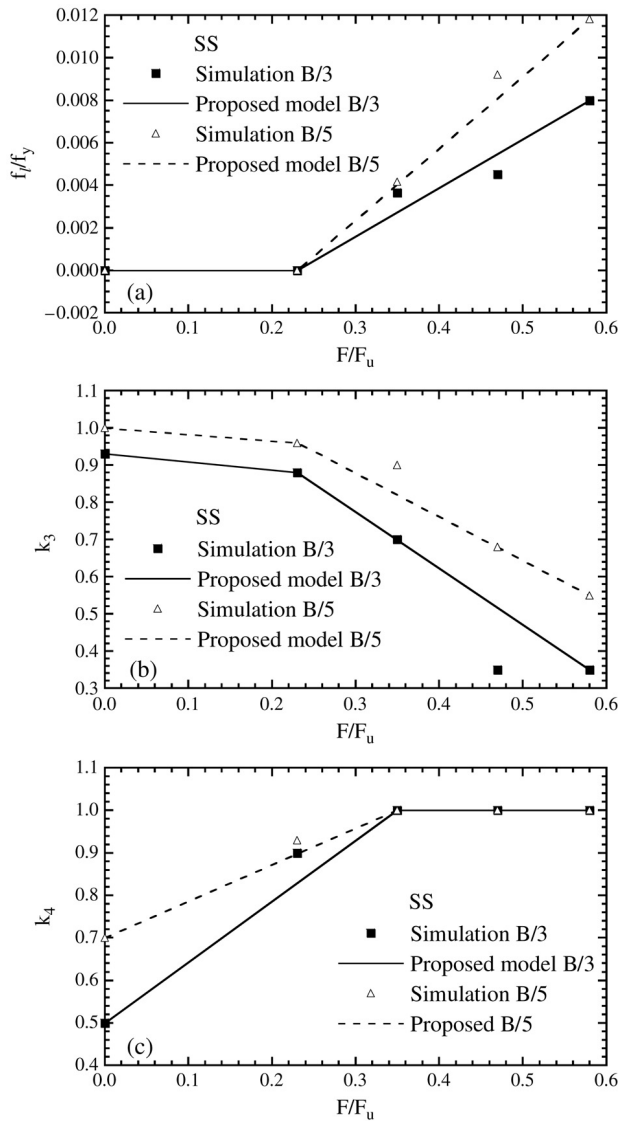


Fig. 15.  $f_i/f_y$ ,  $k_3$  and  $k_4$  versus axial load ratio  $F/F_u$  for CFT columns with SS sections.

the CU section. However, when the spacing of the reinforcing ties is small (e.g. smaller than B/5), the CFT with the SS section may possibly keep up the same  $k_3$  value as a CFT with the CU section. From the results of numerical simulations, the following empirical equations for  $k_3$  may be proposed when the reinforcing ties are at B/3 spacing:

$$k_3 = 0.93 - 0.217(F/F_u), \quad 0 \leq F/F_u \leq 0.23 \quad (16a)$$

$$k_3 = 1.228 - 1.514(F/F_u), \quad 0.23 \leq F/F_u \leq 0.58. \quad (16b)$$

When the reinforcing ties are at B/5 spacing, the following equations may be suggested:

$$k_3 = 1 - 0.174(F/F_u), \quad 0 \leq F/F_u \leq 0.23 \quad (17a)$$

$$k_3 = 1.229 - 1.171(F/F_u), \quad 0.23 \leq F/F_u \leq 0.58. \quad (17b)$$

From Fig. 15(c), we can see that the strength factor  $k_4$  is less than 1 when the axial load ratio  $F/F_u$  is less than 0.35. For the CFT with reinforcing ties at close spacing (e.g. B/5), the strength factor  $k_4$  is usually greater than that for a CFT with reinforcing ties at large spacing (e.g. B/3). By comparing Fig. 15(c) with Figs. 13(c) and 10(c), one can see that with the same axial load ratio, the strength factor  $k_4$  for a CFT with the SS section is larger than that for a CFT with the SU section but smaller than that for a CFT with the CU section. However, when the spacing of the reinforcing ties is small (e.g. smaller than B/5), the CFT with the SS section might possibly maintain the same  $k_4$  value as that with the CU section. On the basis of the results of numerical simulations, the following empirical equations for  $k_4$  may be proposed the when reinforcing ties are at B/3 spacing:

$$k_4 = 0.5 + 1.429(F/F_u), \quad 0 \leq F/F_u \leq 0.35 \quad (18a)$$

$$k_4 = 1, \quad 0.35 \leq F/F_u \leq 0.58. \quad (18b)$$

When the reinforcing ties are at B/5 spacing, the following equations may be suggested:

$$k_4 = 0.7 + 0.857(F/F_u), \quad 0 \leq F/F_u \leq 0.35 \quad (19a)$$

$$k_4 = 1, \quad 0.35 \leq F/F_u \leq 0.58. \quad (19b)$$

Fig. 11(c) shows the typical deformation shapes of the SS-0.35-B/3 column around the ultimate loading stage. It can be observed that the concrete core and steel tube keep in contact with each other like in the case of the CFT with the CU section. Due to the reinforcing ties, no local buckling of the tube takes place. This phenomenon can also be observed for the CFT with the SS section at other axial load ratios and tie spacings [25].

## 5. Conclusions

In this paper, nonlinear finite element analyses of CFT columns with CU, SU and SS sections are analyzed. On the basis of the numerical results, the following conclusions may be drawn:

- (1) The lateral confining pressure  $f_l$  generally increases with the increasing of the axial load ratio  $F/F_u$ . When this axial load ratio is low, the steel tubes provide weak lateral support to the concrete core and the lateral confining pressure  $f_l$  applied to the concrete core may be zero during the subsequent four-point bending loading. When the ratio is high, the steel tubes provide strong lateral support to the concrete core.
- (2) The lateral confining pressure  $f_l$  for a CFT with the SS section is much higher than that for a CFT with the SU section and is of about the same order as that for a CFT with the CU section. The use of reinforcing ties enhances the lateral confining pressure of the tubes. For a CFT with the SS section, the lateral confining pressure  $f_l$  generally increases with the decreasing of the tie spacing.
- (3) For a CFT with the SU section, the concrete core and steel tube cannot keep in contact with each other during the ultimate loading stage due to the weak confining effect;

severe local buckling of the tube takes place at the top and mid-span regions of the column. For CFT columns with CU and SS sections, local buckling is not likely to occur due to the strong confining effect.

- (4) The material degradation parameter  $k_3$  generally decreases with the increasing of the axial load ratio  $F/F_u$ . The material degradation parameter  $k_3$  for a CFT with the SS section is larger than that for a CFT with the SU section but smaller than that for a CFT with the CU section. However, when the spacing of the reinforcing ties is small, the CFT with the SS section may possibly maintain the same  $k_3$  value as a CFT with the CU section.
- (5) When the axial load ratio  $F/F_u$  is low, the concrete cross section cannot maintain the strength  $f'_c$  on average and the strength factor  $k_4$  is smaller than 1. When the axial compressive load is large, the strength factor  $k_4$  is equal to 1 due to the strong confining effect. The strength factor  $k_4$  for a CFT with the SS section is larger than that for a CFT with the SU section but smaller than that for a CFT with the CU section. When the spacing of the reinforcing ties is small, the CFT with the SS section might possibly maintain the same  $k_4$  value as the CFT with the CU section.

## Acknowledgment

This research work was financially supported by the National Science Council, Republic of China, under Grant NSC 90-2625-Z-006-007.

## References

- [1] Furlong RW. Strength of steel-encased concrete beam–columns. *Journal of the Structural Division, ASCE* 1967;93(ST5):113–24.
- [2] Knowles RB, Park R. Strength of concrete filled steel tubular columns. *Journal of the Structural Division, ASCE* 1969;95(ST12):2565–87.
- [3] Ge HB, Usami T. Strength of concrete-filled thin-walled steel box columns: experiment. *Journal of Structural Engineering, ASCE* 1992;118(1):3036–54.
- [4] Ge HB, Usami T. Strength analysis of concrete-filled thin-walled steel box columns. *Journal of Constructional Steel Research* 1994;30(3):259–81.
- [5] Boyd FP, Cofer WF, McLean D. Seismic performance of steel-encased concrete column under flexural loading. *ACI Structural Journal* 1995;92(3):355–65.
- [6] Bradford MA. Design strength of slender concrete-filled rectangular steel tubes. *ACI Structural Journal* 1996;93(2):229–35.
- [7] Shams M, Saadeghvaziri MA. State of the art of concrete-filled steel tubular columns. *ACI Structural Journal* 1997;94(5):558–71.
- [8] Hajjar JF, Molodan A, Schiller PH. A distributed plasticity model for cyclic analysis of concrete-filled steel tube beam–columns and composite frames. *Engineering Structures* 1998;20(4–6):398–412.
- [9] Schneider SP. Axial loaded concrete-filled steel tubes. *Journal of Structural Engineering, ASCE* 1998; 124(10):1125–38.
- [10] Kitada T. Ultimate strength and ductility of state-of-the-art concrete-filled steel bridge piers in Japan. *Engineering Structures* 1998;20(4–6):347–54.
- [11] Roeder CW, Cameron B, Brown CB. Composite action in concrete filled tubes. *Journal of Structural Engineering, ASCE* 1999;125(5):477–84.
- [12] Zhang W, Shahrooz BM. Comparison between ACI and AISC for concrete-filled tubular columns. *Journal of Structural Engineering, ASCE* 1999;125(11):1213–23.

- [13] Uy B. Strength of concrete filled steel box columns incorporating local buckling. *Journal of Structural Engineering*, ASCE 2000;126(3):341–52.
- [14] O’Shea MD, Bridge RQ. Design of circular thin-walled concrete filled steel tubes. *Journal of Structural Engineering*, ASCE 2000;126(11):1295–303.
- [15] Elchalakani M, Zhao XL, Grzebieta RH. Concrete-filled circular steel tube subjected to pure bending. *Journal of Constructional Steel Research* 2001;57(11):1141–68.
- [16] Bradford MA, Loh HY, Uy B. Slenderness limits for filled circular steel tubes. *Journal of Constructional Steel Research* 2002;58(2):243–52.
- [17] Elremaily A, Azizinamini A. Behavior and strength of circular concrete-filled tube columns. *Journal of Constructional Steel Research* 2002;58(12):1567–91.
- [18] Huang CS, Yeh Y-K, Liu G-Y, Hu H-T, Tsai KC, Weng YT, Wang SH, Wu M-H. Axial load behavior of stiffened concrete-filled steel columns. *Journal of Structural Engineering*, ASCE 2002;128(9):1222–30.
- [19] Hu H-T, Huang CS, Wu M-H, Wu Y-M. Nonlinear analysis of axially loaded CFT columns with confinement effect. *Journal of Structural Engineering*, ASCE 2003;129(10):1322–9.
- [20] Hibbit, Karlsson & Sorensen, Inc. ABAQUS/standard user manuals, version 6.2. Providence, RI; 2002.
- [21] Liu G-Y, Yeh Y-K, Tsai KC, Su S-C, Sun W-L. A Study on the behaviors of concrete-filled steel tubular beam–columns subjected to axial load and bending moment, technical report NCREE-03-009, Taipei (Taiwan, ROC); National Center for Research on Earthquake Engineering; 2003 [in Chinese].
- [22] ASCE Task Committee on Concrete and Masonry Structure. State of the art report on finite element analysis of reinforced concrete. New York: ASCE; 1982.
- [23] Mander JB, Priestley MJN, Park R. Theoretical stress–strain model for confined concrete. *Journal of Structural Engineering*, ASCE 1988;114(8):1804–23.
- [24] Richart FE, Brandtzaeg A, Brown RL. A study of the failure of concrete under combined compressive stresses. Bulletin 185. Champaign (IL): University of Illinois Engineering Experimental Station; 1928.
- [25] Chen Z-L. Numerical analysis of concrete filled tubes subjected to combined axial force and moment, M.S. thesis, Tainan (Taiwan, ROC); Department of Civil Engineering, National Cheng Kung University; 2001.
- [26] Saenz LP. Discussion of equation for the stress–strain curve of concrete by Desayi P., Krishnan S. *ACI Journal* 1964;61:1229–35.
- [27] Hu H-T, Schnobrich WC. Constitutive modelling of concrete by using nonassociated plasticity. *Journal of Materials in Civil Engineering*, ASCE 1989;1(4):199–216.
- [28] ACI Committee 318. Building code requirements for structural concrete and commentary (ACI 318-99). Detroit (MI): American Concrete Institute; 1999.
- [29] British Standards Institute. Design of Composite Steel and Concrete Structure, Eurocode 4. London; 1994.